ARTICLES

First-principles total-energy calculations for planar shear and cleavage decohesion processes in *B*2-ordered NiAl and FeAl

N. I. Medvedeva
Institute of Solid State Chemistry, Ekaterinburg, Russia

O. N. Mryasov
Department of Physics and Astronomy, Northwestern University, Evanston, Illinois 60208-3112

Yu. N. Gornostyrev
Institute of Metal Physics, Ekaterinburg, Russia

D. L. Novikov and A. J. Freeman
Department of Physics and Astronomy, Northwestern University, Evanston, Illinois 60208-3112
(Received 1 May 1996)

The fracture and deformation behavior of the ordered NiAl and FeAl intermetallics were studied on the basis of full-potential local-density linear-muffin-tin orbital total-energy calculations of the shear and cleavage decohesion processes. Based on *ab initio* calculations of generalized stacking fault energetics, the structure of the dislocation core was constructed in the scope of the Peierls-Nabarro model with a generalized restoring force law. We found that dislocations in FeAl show a strong tendency for splitting into two superpartials, in contrast with NiAl. Estimates of the Peierls stress yield the correct preferred slip systems for NiAl (i.e., $\langle 100 \rangle \{110\}$) and FeAl (i.e., $\langle 111 \rangle \{110\}$). [S0163-1829(96)00343-8]

I. INTRODUCTION

Aluminides with the *B*2 structure exhibit a wide range of interesting physical and mechanical properties, such as high-ordering temperature, corrosion resistance, and high-temperature strength. The lack of ductility, however, often limits the application of these intermetallic alloys. One may expect many reasons for their low ductility. In accordance with recent understanding, the poor ductility of FeAl is caused mainly by environmental factors (hydrogen-induced embrittlement) (Ref. 1) in contrast to NiAl, which is considered to be intrinsically brittle.[2] However, a recent experiment[3] illustrated that it is possible to achieve high (25%) tensile elongation for high-purity monocrystalline NiAl. It is important to stress that the most intriguing fact observed in Ref. 3 is that, after substantial plastic deformation in NiAl, cleavage fracture takes place. This cleavage-type crack propagation is observed also for FeAl and CoAl.[1,4] Thus these experimental facts demonstrate that the nature of the brittleness in this type of material is still not completely understood.

The principal processes that determine brittleness and/or toughness are dislocation mobility and crack blunting.[5] In the case when the effects of crack shielding can be neglected (for example when the mobility of the dislocations is low), the description of brittle vs ductile behavior in terms of the Rice-Thomson approach[5-7] is based on a comparative analysis of two competing processes: (i) the opening of the crack, and (ii) the emission of a dislocation near the crack tip. Now, the resistance to dislocation emission at a crack tip may be measured by the maximum energy associated with the sliding of atomic planes.[6] This parameter, the so-called unstable stacking fault energy (γ_{us}), is determined by extremal properties of the γ surface, namely, the energy of the generalized stacking fault (GSF) associated with a rigid shift of one-half of the crystal along some direction in the slip plane. The definition of the GSF was introduced by Vitek[8] as an important characteristic for understanding dislocation structure and mobility.

An essential feature of the GSF is that as a planar fault, it is not as complicated an object for modeling as is a dislocation, and so it is quite possible to perform accurate *ab initio* band-structure calculations of its energetics. On the other hand, what may make it useful is that knowledge of the GSF energetics allows one to analyze the structure of a dislocation core in the scope of the Peierls-Nabarro (PN) model[9,10] with general restoring force. Thus the PN model may be considered as a bridge that brings together information offered by *ab initio* band-structure methods and the problem of dislocation core structure. Recently such an approach was used for an analysis of dislocation structure in fcc metals[11] and in Si.[10]

To our knowledge there have been no systematic first-principles calculations of γ surfaces in intermetallic compounds. There are a number of *ab initio* calculations of antiphase boundary energies (APB's), associated with $\frac{1}{2}\langle 111 \rangle \{110\}$ shear in NiAl and FeAl.[12-14] Recently, the peculiarities of NiAl and FeAl fractures were studied on the basis of *ab initio* calculations of cleavage characteristics

by the full-potential linearized-augmented-plane-wave (FLAPW) method.[15]

On the other hand, both the γ surface[16] and dislocation structure[17] were simulated using an atomistic molecular static approach with different types of interatomic potentials. However, there is an open question of whether the potentials used in these atomistic simulations are good enough to describe the essential features of the mixed covalent-ionic bonding in NiAl or FeAl, and whether that type of potential is transferable for other compounds like TiAl.

In this paper, we attempt to explain some features of the mechanical behavior of NiAl and FeAl on the basis of *ab initio* full-potential linear muffin-tin-orbital (FLMTO) (Ref. 18) total-energy calculations for both cleavage and planar shear fault characteristics for possible slip modes. The structure of the dislocation core was constructed based on the solution of the Peierls-Nabarro model with general restoring force determined from *ab initio* calculations of the energy for the unrelaxed GSF. Finally, deformation modes are discussed using results of Peierls stress estimates for NiAl and FeAl.

II. METHODOLOGY AND DETAILS OF THE CALCULATIONS

The first-principles total-energy calculations were performed using the FLMTO method without any shape approximation to the effective crystal potential and charge density.[18] We employ the Ceperly-Alder form of the exchange-correlation potential, a scalar relativistic treatment of the valence electrons, and the linear tetrahedron method for integration over the Brillouin zone.

A. Bulk

Calculations for bulk NiAl and FeAl were performed with a triple-kappa basis $k_1^2 = -0.01$, $k_2^2 = -1.0$, and $k_3^2 = -2.3$ Ry. Muffin-tin radii were chosen to be equal for Ni (Fe) and Al atoms with a crystal space filling ratio of 66.9%. Integration over **k** space was performed using $8 \times 8 \times 8$ regular divisions of each axis in reciprocal space. We found that the equilibrium lattice constants for NiAl ($a_{NiAl} = 2.839$ Å) and FeAl ($a_{FeAl} = 2.811$ Å) are in reasonable agreement with experiment (2.887 and 2.862 Å, respectively) and in excellent agreement with results[19] of FLAPW calculations $a_{NiAl} = 2.81$ Å, $a_{FeAl} = 2.83$ Å (Ref. 14) and $a_{NiAl} = 2.84$ Å, $a_{FeAl} = 2.817$ Å. The underestimation of the equilibrium lattice constants is typical, and is usually explained by errors of the local-density approximation itself, and by neglecting the effect of temperature expansion. All results reported in this paper were obtained with the theoretical value of the lattice constants.

B. Generalized stacking fault

The generalized stacking fault energy is determined as the energy necessary to apply for a rigid shift of one-half the crystal on the vector **u** (fault vector) in a slip plane.[8] Periodic boundary conditions have to be imposed in order to use band-structure methods for calculating the GSF energy, which is then determined as a difference of large total energies for two supercells designed to simulate faults with

u=0 and **u**≠ 0 vectors. Thus special care has to be taken regarding convergence and number of **k** points to keep the same precision of the total energy calculated for different stacking faults vectors **u**.

An important factor is the choice of the supercell geometry, since the size of the supercell should be big enough to exclude interaction of the (periodic) faults; together with the poor convergence in the case of huge supercells, this makes such calculations rather expensive. The way to design the supercell with two constant translation vectors $\mathbf{c}_1$ and $\mathbf{c}_2$ and variable vector $\mathbf{c}_3$ has been described previously.[20] The triclinic supercell is considered instead of the base-centered orthorhombic cell. In this work, we follow the traditional choice of a supercell as a repeated stacking of some layers and keep the mirror plane symmetry. Then, the supercell with tetragonal symmetry consisting of five unit cells (ten layers) was constructed for the GSF in the {100} plane. In case of the {110} plane, an orthorhombic supercell with axes a, $b = a\sqrt{2}$, and $c = 3a\sqrt{2}$ (six layers) was used. This supercell geometry is suitable both for calculations of the shear and cleavage decohesion processes. In our FLMTO calculations, a second energy panel was added to account for the $3p$ semicore states of Fe atoms positioned in the vicinity of the fault plane, since in this region the MT radii have to be reduced in order to avoid their overlap.

As a result, we were able to simulate different slip systems in NiAl and FeAl. Calculations of GSF energies were performed for the full range of the variation of the fault vector **u**; in all, seven points were calculated for each direction. No relaxation effects were considered at this stage of the study. Note that an ''unrelaxed'' γ surface is a kind of model object that nevertheless is very important for the analysis of the dislocation core in terms of the PN approach. Thus, our study is based on the suggestion that the ''unrelaxed'' γ surface allows one to detect essential properties of the deformation behavior, at least in the scope of the PN model aproach, and hence to improve the understanding of mechanical properties.

C. Characteristics of the cleavage fracture

The same type of supercell geometry used for the GSF was employed for calculations of the cleavage fracture characteristics for two crystallographic planes {100} and {110}. The cleavage energy G_c is defined as the energy required to cleave an infinite bulk crystal into two semi-infinite parts, and so is the energy to be applied for the creation of two surfaces. In the supercell approach, G_c is calculated as the total-energy difference per unit surface area.

In the case of the $B2$ structure, the supercell geometry is essentially different for the {100} and {110} planes. The {100} plane consists of only one type of atom (Al or Ni), and so this plane is polar and causes some difficulties in the cleavage energy estimates. An analogous problem arises in calculating polar surfaces and interfaces. These problems are related to the impossibility, in the framework of periodic boundary conditions, of constructing a supercell without an excess of one type of atom, and so such a supercell basically represents some off-stoichiometric compound.[21]

We used the following algorithm to calculate the cleavage energy for the {100} polar plane. Calculations of the total energies for three types of supercells were performed: the
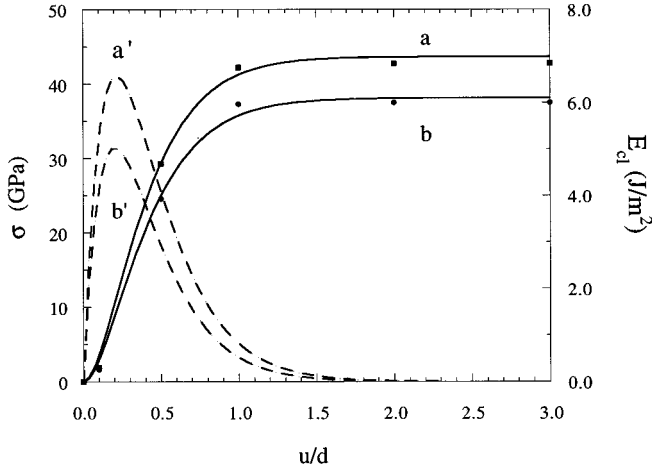
FIG. 1. The energy of separation E_{cl} (J/m^2) and its derivative σ (GPa) as a function of separation distance u (in units of the interplane distance d) counted relative to the equilibrium interplane distance for the {100} plane in NiAl and FeAl. Notations $a(a')$ and $b(b')$ stand for E_{cl} (and derivative σ) for FeAl and NiAl, respectively.

first represents bulk, and consists of seven Ni layers and seven Al layers (E_1); another was constructed from four Ni layers, three Al layers (lack of Al layers), and seven empty layers (E_2); and a third consists of three Ni layers (lack of Ni layers), four Al layers, and seven empty layers (E_3). Then G_c was determined as the total-energy difference of the supercell consisting of seven unit cells (seven Ni layers, seven Al layers) and the sum of the total energies of the last two supercells, $G_c = E_1 - (E_2 + E_3)$. The {110} plane contains both Ni and Al atoms, i.e., it is nonpolar, and in this case G_c was calculated in the usual manner. The energy of separation of two halves of the crystal as a function of distance $E_{cl}(u)$ was then determined by varying the thickness of the vacuum slab.

III. RESULTS AND DISCUSSIONS

A. Cleavage fracture

The calculated dependence of the separation energy on the distance between halves of the crystal $E_{cl}(u)$ for NiAl and FeAl are presented in Fig. 1. As can be seen, at some separation distance this dependence is saturated, and the asymptotic value is the ideal cleavage decohesion energy (G_c). The calculated points in Fig. 1 are approximated with a universal binding energy relation.[22] The maximum derivative of $E_{cl}(u)$ is the so-called theoretical cleavage strength (σ_{max}). Both the cleavage energy G_c and the theoretical strength, σ_{max}, for {100} and {110} planes are presented in Table I. The FLMTO results for G_c are in good agreement with both the earlier FLAPW calculations by Yoo and Fu,[15] and the more recent relaxed results of Wu *et al.*[19] It is also important to stress, that as in Ref. 15 the calculated G_c and σ_{max} are similar for NiAl and FeAl.

An analysis of the dislocation emission process in the scope of the elastic model allows the formulation of criteria[5] (known as Rice-Thompson criteria) of the brittle-ductile transition in the form of the inequality $\mu b / \gamma < 7.5 - 10$,

TABLE I. Cleavage fracture parameters [G_c (J/m^2), σ_{max} (GPa)] and cracking criteria $b\mu / \gamma$.

Alloy	Plane	G_c (J/m^2)	σ_{max} (GPa)	$b\mu / \gamma$
NiAl	{100}	5.7	34	11.7
	{110}	4.15	22	16.1
FeAl	{100}	6.70	42	10.7
	{110}	5.57	26	12.9

where $\gamma = G_c / 2$ is the surface energy and b is the magnitude of the Burgers vector. The process of dislocation emission was studied in a more consistent way by Shoeck[23] with the use of Peierls-Nabarro model approximations. According to Ref. 23, if the inequality

$$\frac{\omega}{b} < 0.94 \frac{(1 - \nu \cos^2 \phi)^2 \mu b}{8 \pi \beta^2 (1 - \nu) \gamma} \tag{1}$$

is true, then brittle propagation of crack should be expected. Here ω is the width of the dislocation core, $\beta = \sin(\phi)\sin(\theta/2)\cos(\theta/2)$, where θ is the angle between the slip plane of the emitted dislocation and the plane of the crack propagation, and ϕ is the angle between the Burgers vector and the direction parallel to the tip of the crack. Equation (1) is analogous to the Rice-Thomson criterion, but in addition takes into account the dislocation core width. The shear modulus μ_{nu} with shear vector $\mathbf{u}$ on a plane with normal vector $\mathbf{n}$, in the case of $\langle 100 \rangle$ slip in {100} or {110} planes, coincides with the c_{44} elastic constant. The calculated ratio $\mu b / \gamma$ for NiAl and FeAl alloys was found to be similar and unexpectedly large (see Table I). This result shows that in terms of this simple criterion both materials have a tendency for brittle propagation of crack.

As mentioned in the Introduction, it was recently observed for pure NiAl monocrystal samples that cleavage fracture takes place after substantial plastic deformation.[3] In accordance with the results of our calculations, the cleavagelike type of the crack tip propagation may be explained by a relatively small value of the surface energy (Table I). As seen in Table I, in terms of Rice-Thomson criteria, one may expect a similar fracture behavior for NiAl and FeAl.

It is interesting to compare results for NiAl and FeAl with those for fcc metals. Among fcc metals such a large value of the $\mu b / \gamma$ ratio is known only for Ir (about 12), whereas for Cu and Ni this value is about 5–7.[11] Note that, among fcc metals, only Ir shows a cleavage fracture after substantial plastic deformation.[24] The analysis presented in Ref. 11 shows that this peculiarity of the Ir fracture is mainly related to the large value of $\mu b / \gamma$.

The segregation of light gas impurities on the crack tip, especially for H impurities, was found to result in a substantial decrease of the cleavage energy in FeAl.[15] However, in the case when brittle propagation of crack takes place, the plasticity of materials is governed by conditions of the crack formation. These conditions are easier to fulfill if gas impurities are segregated or interstitial phases are formed. The latter is most probably a major factor controlling enviromental brittleness of the FeAl.
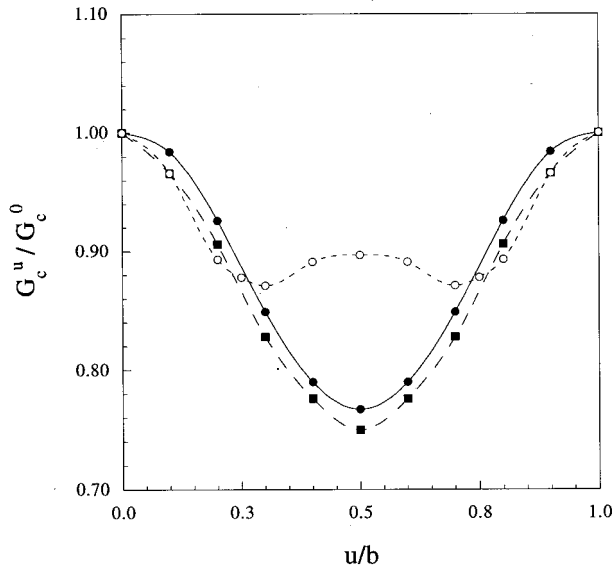
FIG. 2. Dependence of the cleavage energy ratio G_c^u/G_c^0 on the fault vector introduced on the cleavage surface in NiAl for the following: {100} plane and $\mathbf{u}=a\langle100\rangle$, solid line with filled circles; {110} plane and $\mathbf{u}=a\langle100\rangle$, long dashed line with filled squares; and {110} plane and $\mathbf{u}=a\langle111\rangle$, short dashed lines with open circles.

Finally, we also calculated the cleavage decohesion energy G_c^u, which is defined as the cleavage energy in the presence of a planar fault with shear vector $\mathbf{u}$, introduced before separation in a cleavage plane. Results of the calculated dependences of G_c^u on the fault vector modulus (u) for NiAl are presented in Fig. 2. As expected, the cleavage energy is lowered with the appearance of a fault; in particular, the most pronounced lowering was found for $\mathbf{u}=a/2\langle100\rangle$ on the {011} plane (from 4.15 to 3.1 J/m^2) and for $\mathbf{u}=a/2\langle100\rangle$ on the {100} plane (from 5.7 to 4.3 J/m^2). This lowering of the $a/2\langle111\rangle\{011\}$ APB is not so pronounced as for other faults, from 4.15 to 3.95 J/m^2. Thus one should not expect that the APB may be that surface plane in which the opening of a crack is preferable.

B. Shear strength

Another important parameter of fracture is the shear strength σ_{sh}, and the energy of an unstable stacking fault γ_{us}. In accordance with the recently suggested modification of the brittle-ductile transition criterion,[6] brittle propagation of the crack should be expected if the inequality

$$\gamma_{\text{us}} < f(\theta)\gamma \qquad (2)$$

is not true; here $f(\theta)$ is a geometrical factor. The energy γ_{us} is defined as the maximum of the GSF, and scales with the energy necessary for emission of dislocations from the crack.

We calculated GSF energies corresponding to the most important slip modes in NiAl and FeAl. In order to approximate the calculated $E(u)$, and to determine the γ surface, we used Fourier expansions over ($\mathbf{K_n}$) vectors in the two-dimensional lattice which is reciprocal to the slip plane. The form of this expansion is
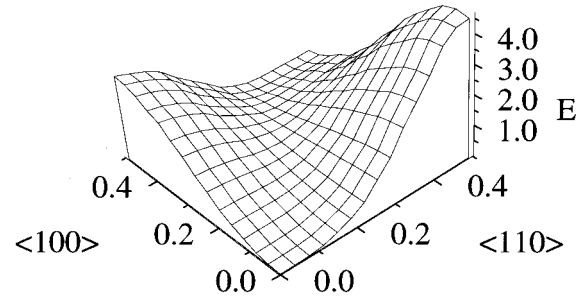
FIG. 3. γ surface for the (110) plane in NiAl (the energy E in J/m^2). The X axis is taken along the $\langle100\rangle$ direction, and the Y axis along $\langle110\rangle$.

$$E(\mathbf{u})=\sum_{n=1} C_n(1-\cos(\mathbf{K}_n\mathbf{u})), \qquad (3)$$

where $\mathbf{K}_n=n_1\mathbf{k}_1+n_2\mathbf{k}_2$, and n_1 and n_2 are integers. For the {110} plane, with X and Y axes along $\langle100\rangle$ and $\langle110\rangle$ respectively, we have $\mathbf{k}_1=(2\pi/b_1)(1,0)$ and $\mathbf{k}_2=(2\pi/b_2)(0,1)$, with $b_1=a$ and $b_2=2\sqrt{2}a$ (where a is a lattice constant). The expansion in Eq. (3) is restricted to terms with $|K_n|\leq2k_1$, and the coefficients C_n are determined using a mean least-squares fit to the calculated energies. The γ surface for the {110} plane in NiAl determined in this way is presented in Fig. 3, and calculated sections are presented in Fig. 4. The maximum GSF (γ_{us}) energies were found at a displacement $u=b/2$ for $\langle100\rangle$ and at $u=0.25b$ for NiAl and $u=0.3b$ for FeAl in the case of $\langle111\rangle$ {110} slip; the corresponding calculated $\gamma/\gamma_{\text{us}}$ ratios are presented in Table II. Note that for all calculated slip modes this ratio is small, and typical for materials with intrinsic brittleness. For example, Ir, which shows cleavage structure, has the ratio $\gamma/\gamma_{\text{us}}=3.8$ according to embedded-atom-method calculations at the same time that for Cu and Ni this ratio is about 11.8 and 8.4, respectively.[7] Thus calculated shear and cleavage characteristics show that both for NiAl and FeAl, cleavage-type crack propagation should be expected. This conclusion is based on the criterion in Eq. (2), with unrelaxed values for γ_{us}. The lattice relaxation may result in a substantial decrease of the corresponding values as demonstrated by recent FLAPW calculations[19] for the {100} slip plane, which means an easier emission of the dislocations from the crack tip. However, even for a 2–3 times decrease of the γ_{us} (Ref. 19) in the case of a noncompact {100} plane, the ratio $\gamma/\gamma_{\text{us}}$ is still small, and the conclusion about cleavagelike crack propagation obtained in terms of Eq. (2) remains valid.

The local minimum on curves c and d in Fig. 4 at $\frac{1}{2}\langle111\rangle$ displacement in the {110} plane corresponds to the APB. We found an APB energy $\zeta_{\text{APB}}=1000$ mJ/m^2 for NiAl, and 765 mJ/m^2 for FeAl is in good agreement with results for unrelaxed APB energies obtained by Fu and Yoo[14] using the FLAPW method (1000 and 650 mJ/m^2). It should be stressed that, in accordance with Ref. 14, relaxation results in a lowering of the APB energy with about a 20% decrease for NiAl and especially for FeAl (from 650 to 300 mJ/m^2).
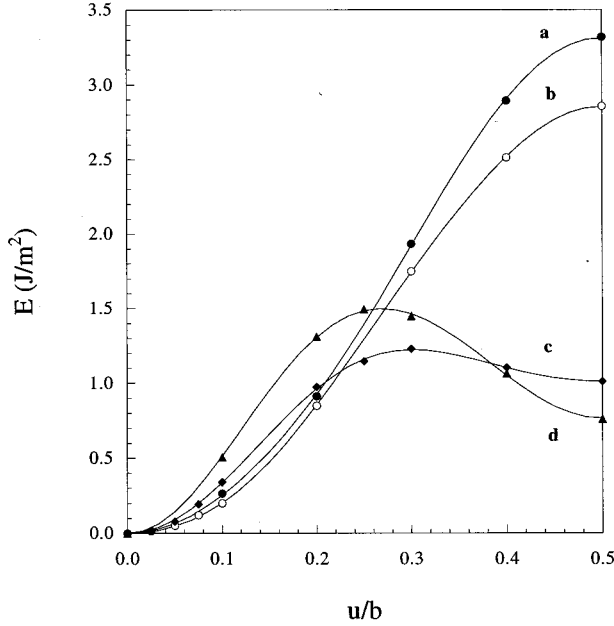
FIG. 4. The energy of the GSF (J/m^2) for the slip systems: (a) $\langle 100 \rangle$ $\{100\}$; (b) $\langle 100 \rangle$ $\{110\}$; and (c); $\langle 111 \rangle$ $\{110\}$, all for NiAl; and (d) $\langle 111 \rangle$ $\{110\}$ for FeAl.

The shear modulus μ_{nu} can also be determined from the GSF energies for a plane with normal vector **n** and displacement vector **u**. Assuming that interactions in the crystal are restricted to nearest neighbors, a simple relation between GSF energies $E(\mathbf{u})$ (for small **u**) and corresponding shear moduli μ_{nu} can be found. The restoring force $dE(\mathbf{u})/d\mathbf{u}$ acting between halves of the crystal can be expressed through the shear deformation ε and shear moduli μ_{nu}, in accordance with Hooke's law

$$\frac{dE(\mathbf{u})}{d\mathbf{u}} = 2\mu_{nu}\varepsilon = \mu_{nu}\frac{u}{d}. \tag{4}$$

Then we have the following expression for estimates of the shear moduli:

$$\mu_{nu} = d\frac{d^2 E(\mathbf{u})}{d\mathbf{u}^2}, \tag{5}$$

where d is the interplane distance. Thus, Eq. (5) allows a rough estimate of the shear moduli using the calculated GSF energies. Results of such estimates are presented in Table III along with experimental data. As can be seen from Table III, the theoretical values for μ_{nu} are in reasonable agreement

TABLE II. Shear strength σ_{sh} (GPa) and cracking criteria σ_{max}/σ_{sh}, γ/γ_{us}.

Alloy	Plane and shear vector	σ_{sh} (GPa)	$\sigma_{sh}^{exp}/\mu_{nu}$	σ_{max}/σ_{sh}	γ/γ_{us}
NiAl	$\{100\}$ $\langle 100 \rangle$	37.5	0.32	0.8	0.91
	$\{110\}$ $\langle 100 \rangle$	31.3	0.27	0.96	0.91
	$\{110\}$ $\langle 111 \rangle$	13.3	0.10	2.25	2.15
FeAl	$\{110\}$ $\langle 111 \rangle$	18.1	0.33	1.93	1.85

TABLE III. Shear moduli estimated from GSF energies calculated for NiAl and FeAl.

Alloy	Plane and shear vector	μ_{nu}(exp),GPa	μ_{nu} (theor),GPa
NiAl	$\{100\}$ $\langle 100 \rangle$	116	92
	$\{110\}$ $\langle 100 \rangle$	116	92
	$\{110\}$ $\langle 111 \rangle$	41	61
FeAl	$\{110\}$ $\langle 111 \rangle$	55	87

with experimental data even if Eq. (5) is very approximate. It is also important to note that shear moduli estimated in this way do not reflect the experimentally observed degree of anisotropy of the elastic response in NiAl. Obviously this result may be related also with the above-mentioned approximations.

It is seen in Table II that the results for $\sigma_{sh}/\mu_{nu}^{exp}$ are systematically larger than those obtained by molecular dynamics calculations for metallic alloys.[25] This is undoubtedly related to the neglect of relaxation in our model, which was especially clearly revealed in the small value of the ratio σ_{max}/σ_{sh}, which was found to be less than 1 for $\langle 100 \rangle$ shear. As is known (see, for example, Ref. 26), for all metals the cleavage strength is larger than the shear strength. Nevertheless, we assume in this stage of our study that a model without relaxation can correctly reproduce the relation between σ_{sh} for different displacements. The smallest value of the ideal shear strength was found for NiAl in the case of $\langle 111 \rangle$ $\{110\}$ shear (see Fig. 1). Hence one may conclude that the deformation in NiAl is related mainly to $\langle 111 \rangle$ dislocations. However, this conclusion contradicts experimental results,[2] which show that the $\langle 111 \rangle$ $\{110\}$ deformation mode is most unlikely in this alloy and $\langle 100 \rangle$ are the most preferable modes. The solution of this problem in terms of the PN model is discussed in Sec. III C.

C. Construction of the dislocation core

We concentrate on the analysis of deformation modes and dislocation structure in the scope of the PN model. As is known,[27] in terms of the PN model the crystal lattice in both upper and lower half-spaces (with respect to the slip plane) is considered as an elastic continuum which is characterized by elastic displacements. The upper and lower half-spaces are restricted correspondingly by planes A (from below) and B (from above). Then the distribution of the elastic displacements in the PN model is determined by the balance of the lattice restoring forces acting between planes A and B, and elastic stresses of the continuum media represent the rest of the crystal.

The displacements in the A (or B) plane parallel to the Burgers vector are described by the PN equation[27]

$$2\frac{\mu D}{\pi}\int_{-\infty}^{\infty}\frac{d\xi}{\xi - x}\frac{du^A(\xi)}{d\xi} = -\frac{dE(u)}{du}, \tag{6}$$

where E is the energy of interaction (per unit area) between the upper and lower parts of the lattice as a function of the relative displacement u, which is related to the absolute displacement u^A by the simple relation $\mathbf{u} = 2u^A$
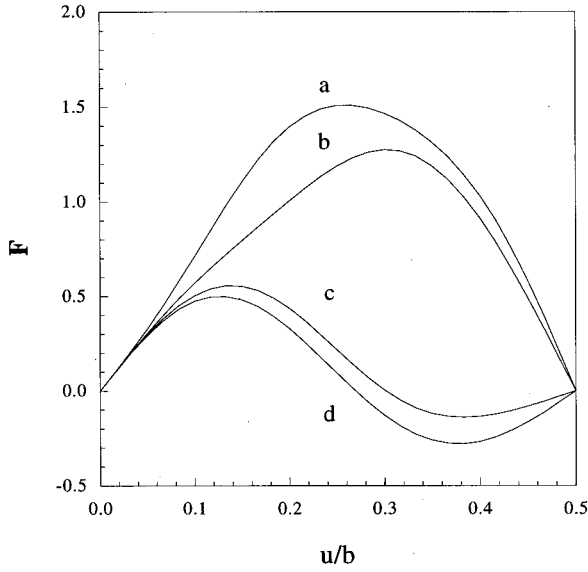
FIG. 5. Restoring force F [in units of $(4\pi\omega_0/\mu Db)(dE/du)$] as a function of displacement u/b for slip systems (a) $\langle 100\rangle$ $\{110\}$; (b) $\langle 100\rangle$ $\{100\}$; and (c) $\langle 111\rangle$ $\{110\}$ all for NiAl, and (d) $\langle 111\rangle$ $\{110\}$ for FeAl.

$+\operatorname{sgn}(x)\cdot\mathbf{b}/2$;[27] D is a parameter equal to 1 for screw dislocation, and to $1/(1-\nu)$ for edge dislocation.

One should point out two problems appearing in the analysis of the dislocation core structure in the scope of the PN model: (i) the restoring force law is unknown, and (ii) the mainly mathematical problem related to the solution of the nonlinear integral equation, Eq. (6). To determine the restoring force law we use results of the GSF total-energy calculations. Restoring forces determined in this way for NiAl and FeAl are presented in Fig. 5.

The solution of the PN model Eq. (6) for an arbitrary restoring force law is unknown. In the *original* PN model only the lowest harmonic of the Fourier expansion of $E(\mathbf{u})$ is considered, so that the restoring force is taken to be proportional to $\sin(4\pi u^A/b)$. In this case the solution is well known[27] as

$$u^A=-\frac{b}{2\pi}\arctan\frac{x}{\omega_0}, \qquad (7)$$

where $\omega_0=dD/2$ is the width of the dislocation core. Later Foreman, Jaswon, and Wood (FJW) proposed a solution for the more general case.[28] An effective method to find the solution of the PN equation, $u(x)$, for a wide class of $E(\mathbf{u})$ functions was proposed by Lejcek.[29] In the following analysis we use his formalism.

In accordance with Ref. 29, Eq. (6) is considered as an example of a Hilbert transformation, so that the density of the infinitesimal dislocation $\rho(x)=du(x)/dx$ may be written in the form

$$\rho(x)=\sum_{k=1}^{N}\sum_{n=1}^{p_k}\rho_{nk}(x), \qquad (8)$$

with restoring force

$$\frac{2}{\mu D}\frac{dE(u(x))}{dx}=\sum_{k=1}^{N}\sum_{n=1}^{p_k}g_{nk}(x), \qquad (9)$$

where

$$\rho_{nk}=\frac{1}{2}\left[\frac{A_{nk}}{(x-z_k)^n}+\frac{\overline{A}_{nk}}{(x-\overline{z}_k)^n}\right] \qquad (10)$$

and

$$g_{nk}=-\frac{i}{2}\left[\frac{A_{nk}}{(x-z_k)^n}-\frac{\overline{A}_{nk}}{(x-\overline{z}_k)^n}\right] \qquad (11)$$

are real and imaginary parts of some analytic function; N is the number of the poles of order p_k at the points $z_k=x_k+i\zeta_k$ $(k=1,\ldots,N)$. If the dislocation is split, then x_k gives the positions of the partial dislocations, and ζ_k gives the width of the dislocation core.

We consider here two types of dislocations, namely edge dislocations with Burgers vector $\langle 111\rangle$ and $\langle 100\rangle$. It is sufficient to use parameters $N=1$ and $p_k=3$ in the case of $\langle 100\rangle$ dislocations, and $N=2$ and $p_k=2$ for $\langle 111\rangle$ dislocations. Using Eqs. (8)–(11) one can obtain expressions for displacements $u(x)$ and restoring forces $\partial E/\partial u$ in convenient parametric forms

$$\frac{2\pi u(\theta)}{b}=\frac{1}{2}\left[\theta_1+\theta_2-\frac{\alpha-1}{\alpha}(\sin\theta_1+\sin\theta_2)\right], \qquad (12)$$

$$\frac{4\pi\omega_0}{\mu Db}\frac{\partial E}{\partial u}=\frac{1}{2\alpha}\left[\sin\theta_1+\sin\theta_2+2\frac{\alpha-1}{\alpha}\right.$$
$$\left.\times\left(\sin^2\frac{\theta_1}{2}\sin\theta_1+\sin^2\frac{\theta_2}{2}\sin\theta_2\right)\right] \qquad (13)$$

for $\langle 111\rangle$ dislocations, and

$$\frac{2\pi u(\theta)}{b}=\theta-\frac{\alpha-1}{\alpha}\sin\theta-\beta\sin\theta, \qquad (14)$$

$$\frac{4\pi\omega_0}{\mu Db}\frac{\partial E}{\partial u}=\frac{1}{\alpha}\left[\sin\theta+2\frac{\alpha-1}{\alpha}\sin^2\frac{\theta}{2}\sin\theta\right.$$
$$\left.+2\sin^3\frac{\theta}{2}\beta\cos 3\theta/2\right] \qquad (15)$$

for $\langle 100\rangle$ dislocations, where

$$\theta_1(\theta)=2\operatorname{arccot}\frac{x-\delta}{\zeta}, \qquad \theta_2(\theta)=2\operatorname{arccot}\frac{x+\delta}{\zeta},$$

$$\theta=2\operatorname{arccot}\frac{x}{\zeta}.$$

Here we assumed that superpartial dislocations are at $\pm\delta$, and have the same core width $\zeta=\alpha\omega_0$.

The earlier proposed solutions of the PN equation can be obtained as limiting cases of Eqs. (12)–(15). In particular, for $\delta=0$ and $\theta_1=\theta_2$ we have expressions equivalent to the FJW solution, and if, in addition, $\alpha=1$, then expressions Eqs. (12)–(15) are transformed to the original solution of the PN model [see Eq. (7)].

TABLE IV. Dislocation core structure parameters (α, β_1, δ) and Peierls stress σ_P.

Alloy	Slip plane and Burgers vector	α	β	δ, a	$\sigma_P^{(edge)}/\mu$	$\sigma_P^{(edge)}$ MPa
NiAl	$\{100\}\langle100\rangle$	1.0	-0.3	0.0	0.057	5240
	$\{110\}\langle100\rangle$	1.47	-0.71	0.0	0.0075	690
	$\{110\}\langle111\rangle$	1.86	0.0	0.84	0.072	4800
FeAl	$\{110\}\langle111\rangle$	1.81	0.0	1.64	0.0058	510

We now consider only an analysis of the edge dislocations, for which the PN model is expected to be most adequate. The parameters α, β, and δ, determined from the fit to the curves presented in Fig. 4 using Eqs. (12) and (13) or (14) and (15), are presented in Table IV. Dislocations with $\mathbf{b}=a\langle100\rangle$ have a compact core and are not split into dislocations with a smaller b ($\delta=0$). The tendency of the splitting into two superpartials for the dislocation with $\mathbf{b}=a\langle111\rangle$ is quite obvious (see Table IV), and the distribution of the displacements $u^A(x)$ determined with the use of Eq. (12) for NiAl and FeAl are presented as Fig. 6. As is clearly seen, $\langle111\rangle$ dislocations in FeAl demonstrate an appreciable tendency for splitting ($\delta_{FeAl}=1.64a$); at the same time, in NiAl the distance between superpartials is the order of the width of their core.

In the scope of continuum elastic theory, the width of the splitting is proportional to $\delta\sim\mu b_{sp}^2/\zeta_{APB}$, i.e., it increases with lowering of the APB energy. On the other hand, the calculated unrelaxed APB energy ζ_{APB} for FeAl is slightly smaller that for NiAl, but the splitting of a $\langle111\rangle$ dislocation in FeAl is two times larger (see Table IV). Hence, in contrast to elastic theory, in terms of the PN model the splitting is determined not only by the APB energy, but also by the shape of corresponding section of the γ surface.

Let us now consider the Peierls stress σ_P for different types of dislocations. Following Nabarro,[30] the magnitude of σ_P may be determined if one assumes that the field of the
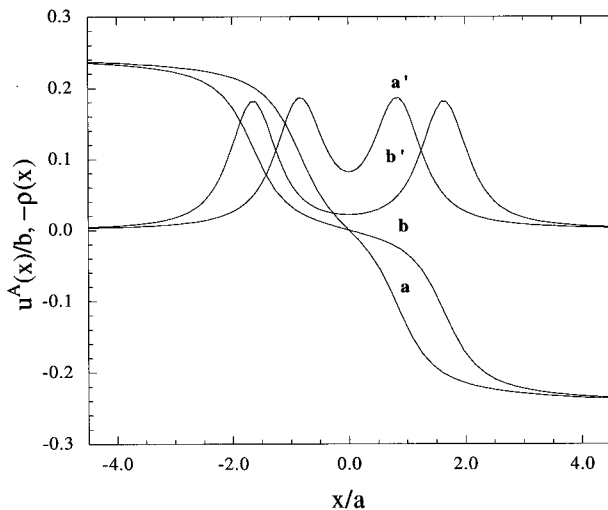
displacements $u(x-l)$ does not depend on the position of the center of the dislocation l. Then, by calculating the so-called ''misfit energy'' per unit length of dislocation

$$\Phi_P(l)=S_0\sum_n E(u(x_n-l)) \quad (16)$$

(where the sum is performed for the positions of atomic arrays x_n, which are parallel to the dislocation axis and S_0 is the area per atom), we have

$$\sigma_p=\frac{1}{b}\left[\frac{d\Phi_P(l)}{dl}\right]_{max}. \quad (17)$$

The sum over n can be simplified using the Poisson formula

$$\Phi_P(l)=S_0\sum_{s=-\infty}^{s=\infty}\int_{-\infty}^{\infty}E(u(ht-l))\exp(2\pi ist)dt$$
$$=S_0\sum_{s=-\infty}^{s=\infty}\exp^{2\pi isl/h}J(s), \quad (18)$$

where

$$J(s)=\frac{-1}{2\pi is}\int_{-\infty}^{\infty}\frac{\partial E(u)}{\partial u}\frac{\partial u}{\partial x}\exp(2\pi isx/h)dx, \quad (19)$$

and h is the period of the lattice in the direction perpendicular to the dislocation line in the slip plane. In Eq. (18) it is sufficient to consider lowest harmonic contributions. Then, if the parity properties of dE/du and du/dx are taken into account, we have

$$\Phi_P(l)=\Phi_P^{(0)}+2S_0\cos(2\pi l/h)J(1) \quad \text{and}$$

$$\sigma_p=\frac{4\pi S_0}{bh}J(1), \quad (20)$$

and the problem is reduced to integrating products of analytic functions [Eqs. (10) and (11)]. The values of σ_P determined in this way are given in Table IV. For NiAl, the lowest value of σ_P corresponds to the slip system $\langle100\rangle\{011\}$. Note that the $\langle111\rangle\{011\}$ dislocations, for which GSF energy barriers are minimal (see Fig. 6), have large values of σ_P. The latter is easy to understand on the basis of the analysis performed above. Naturally, the magnitude of σ_P is controlled not only by the energy barrier for homogeneous shear, but also by the size of the area where most appreciable lattice distortions are taking place and by the character of the distribution of the distortions. Since $a\langle111\rangle$ dislocation in NiAl is almost not split, distortions in the area of the core are large and it is hard to move this dislocation over the lattice. For FeAl, since the $a\langle111\rangle$ dislocation is split into $a/2$ $\langle111\rangle$, with a smaller dislocation Burgers vector than the original, the Peierls stress in FeAl is controlled by the mobility of those superpartial dislocations.

The displacement of atoms in a direction perpendicular to the slip plane is not treated in the PN model. Thus the effect of relaxation on the mobility of dislocations cannot be ana-

FIG. 6. Structure of the dislocation core; distribution of displacements, $u^A(x)/b$ and the density of infinitesimal dislocation $\rho(x)$ for NiAl (curves a and a') and for FeAl (curves b and b').

lyzed by a simple replacement of the unrelaxed $E(u)$ dependence by the relaxed one. The role of the relaxation can be qualitatively estimated by a comparison of the difference $\Delta E = E_{\text{unrelaxed}} - E_{\text{relaxed}}$, with the energy of the elastic distortion $\mu \varepsilon_{\text{rel}}^2 L$ induced by displacement of atoms in the dislocation core. The second parameter $\varepsilon_{\text{rel}}^2$ is the lattice deformation in a process of relaxation and $L \sim b$ is a typical size of the area with considerable relaxation in direction perpendicular to the slip plane. In case $\Delta E \ll \mu \varepsilon_{\text{rel}}^2 L$, the role of relaxation is neglegible; if those parameters are of the same order, one may expect that value of σ_p to decrease rather considerably as a result of such a relaxation. However, we do not expect this to change the qualitative conclusions, since a substantial decrease of the ζ_{APB} in FeAl (Ref. 14) only would increase the width of the splitting and, correspondingly, a further lowering of the Peierls stress σ_p in FeAl should be expected. On the other hand, the lowering of the ζ_{APB} for NiAl is too small for a splitting of the dislocation and so the Peierls stress is expected to remain rather high.

Our analysis supports a suggestion that the APB energy is a very important parameter that controls the slip mode behavior of $B2$-ordered alloys.[31] However, the particular value of σ_P for different slip systems depends on details of the restoring force law which is itself controlled by details of the chemical bonding, or even more importantly by anisotropy of the chemical bonding. This conclusion can also be illustrated by the fact that estimates of σ_P performed in the scope of the analysis described above differ from the original PN approximations estimates by an order of magnitude.

IV. SUMMARY AND CONCLUSIONS

For NiAl and FeAl ordered alloys, all-electron *ab initio* local-density calculations of the γ-surface sections and corresponding characteristics of the shear and cleavage decohesion processes were performed. We found that the cleavage energies (G_c) determined with the FLMTO method are in a good agreement with earlier FLAPW results by Fu and Yoo.[14] The results of our calculations of cleavage characteristics show that both in NiAl and FeAl the habit crack plane is {110} which agrees with experimental observations for NiAl. It was shown for a Fe$_{60}$Al$_{40}$ alloy that the {100} cleavage plane is preferable.[4] Possible reasons for such a contradiction were discussed by Yoo and Fu,[15] and related to a mutual orientation of crack and operative slip planes. The calculated ratio $\mu b / \gamma$ is fairly large (greater than 10), which, according to the simple Rice-Thomson criterion, indicates a tendency to brittle propagation of the crack in both materials (cf. Sec. III A). The same conclusion was also drawn (cf. Sec. III B) on the basis of an analysis of the theoretical shear strength σ_{sh} and unstable stacking fault γ_{us} data. Thus first-principles calculations show that the mechanism of the intrinsic brittleness both for NiAl and FeAl is likely to be related with cleavage-type crack propagation. This is consistent with recent experimental studies of the fracture in these intermetallics at room temperature.[4,3] However, to understand the physical mechanisms driving the difference in tensile ductility of those two alloys, one has to address questions not only about crack propagation but also about crack nucleation processes, which depends on many factors, first of all on the mobility of dislocations.

Based on *ab initio* calculations, the structure of the dislocation cores were determined using solutions of the PN model for a general restoring force. We found that (i) the core of a $\langle 100 \rangle$ dislocation is compact, in agreement with high-resolution transmission electron microscopy measurement by Mills and Miracle;[32] and (ii) a $\langle 111 \rangle$ dislocation is split into two superpartial $a/2 \langle 111 \rangle$ dislocations. The distance of the splitting in NiAl is about the width of the dislocations, but is much larger in FeAl. Estimates of the Peierls stress in terms of this approach allowed us to reproduce correctly the relation between slip systems ($\langle 100 \rangle$ {100} in NiAl, and $\langle 111 \rangle$ {110} in FeAl). Our calculations and analysis show, in agreement with the original work of Rachinger and Cottrell,[31] that the main factor making unlikely the appearance of $\langle 111 \rangle$ {110} slip in NiAl is the high APB energy in this alloy, although the shape of the γ surface also contributes considerably to the structure of the dislocation core. In accordance with our results, compared with NiAl, the relatively low Peierls stress in FeAl, and the correspondigly higher mobility of the dislocations, is likely to be the main intrinsic factor why FeAl shows a better tensile ductility than NiAl.[4] We expect that a proper treatment of relaxation will result in some lowering of the Peierls stress, but will not change the qualitative conclusions obtained here.

Finally, our results show that first-principles total-energy calculations of the γ surface and shear characteristics in combination with the PN model analysis provide a reasonable basis for a theoretical study of the dislocation structure and operative slip modes in $B2$ intermetallic compounds. We conclude that this approach would be especially useful in the study of materials for which models of interatomic interactions are not accurate enough or justified, e.g., for γ-TiAl.

ACKNOWLEDGMENTS

[1] C. T. Liu, in *Ordered Intermetallics - Physical Metallurgy and Mechanical Behaviour*, NATO ASI, NATO Science Committee, edited by C. T. Liu, R. W. Cahn, and G. Sauthoff (Kluwer Academic, Dordrecht, 1992).

[2] R. D. Noebe, R. R. Bauman, and N. V. Nathal, Int. Mater. Rev. **38**, 34 (1993).

[3] V. I. Levit, I. A. Bul, J. Hu, and M. J. Kaufman, Scripta Metall. Mater. **34**, 1925 (1996).

[4] K. M. Chang, R. Darolia, and H. A. Lipsitt, in *High Temperature Ordered Intermetallic Alloys IV*, edited by L. Johnson, D. P. Pope, and J. O. Stiegler, MRS Symposia Proceedings No. 213 (Materials Research Society, Pittsburgh, 1991), p. 957.

[5] J. R. Rice and R. Thomson, Philos. Mag. **73**, 29 (1973).

[6] Y. Sun, J. R. Rice, and L. Trushinovsky, in *High Temperature Ordered Intermetallic Alloys IV* (Ref. 4), p. 243.

[7] J. R. Rice, J. Mech. Phys. Solids **40**, 239 (1992).

[8] V. Vitek, Cryst. Latt. Def. **5**, 1 (1974).

[9] E. Kaxiras and M. S. Duesbery, Phys. Rev. Lett. **70**, 3752 (1993).

[10] B. Joos, Q. Ren, and M. S. Duesbery, Phys. Rev. B **50**, 5890 (1994).

[11] Y. N. Gornostyrev, M. I. Katsnelson, A. G. Mihin, Yu. N. Osetskii, and A. V. Trefilov, Phys. Met. Metall. **77**, 45 (1994).

[12] T. Hong and A. J. Freeman, Phys. Rev. B **43**, 6446 (1991).

[13] T. Hong and A. J. Freeman, J. Mater. Res. **7**, 68 (1992).

[14] C. L. Fu and M. H. Yoo, in *High Temperature Ordered Intermetallic Alloys IV* (Ref. 4), p. 667.

[15] M. H. Yoo and C. L. Fu, Mater. Sci. Eng. A **153**, 470 (1993).

[16] D. Farkas and C. Vailhe, J. Mater. Res. **8**, 3050 (1993).

[17] T. A. Parthasathy, S. I. Rao, and D. M. Demiduk, Philos. Mag. A **67**, 643 (1993).

[18] M. Methfessel, Phys. Rev. B **38**, 1537 (1988).

[19] R. Wu, L. Zhong, L. Cheng, and A. J. Freeman, Phys. Rev. B (to be published).

[20] A. T. Paxton, in *Electron Theory in Alloy Design*, edited by D. G. Pettifor and A. H. Cottrell (Alden, Oxford, 1992), Chap. XX.

[21] W. R. L. Lambrecht, C. Amador, and B. Segal, in *Application to Multiple Scattering Theory to Materials Science*, edited by W. H. Bolter, P. H. Dederichs, A. Gonis, and R. Weaver, MRS Symposia Proceedings No. 253 (Materials Research Society, Pittsburgh, 1993), p. 381.

[22] J. H. Rose, J. R. Smith, and J. Ferrante, Phys. Rev. B **28**, 1835 (1983).

[23] G. Schoeck, Philos. Mag. A **63**, 111 (1991).

[24] C. A. Brookes, J. H. Greenwood, and J. L. Routbort, J. Inst. Metall. **4**, 109 (1970).

[25] N. H. Macmillan, in *Atomistics of Fracture*, edited by R. Lataninson and J. R. Pickens (Plenum, New York, 1983), pp. 95–164.

[26] R. Thomson, in *Atomistics of Fracture* (Ref. 25), pp. 167–204.

[27] J. Hirth and J. Lote, *Theory of dislocation*, McGraw-Hill Series in Material Science and Engineering (McGraw-Hill, New York, 1968).

[28] A. J. Foreman, M. A. Jaswon, and J. K. Wood, Proc. Phys. Soc. **64A**, 156 (1951).

[29] D. Lejcek, Czech. J. Phys. B **26**, 294 (1976).

[30] F. R. Nabarro, Adv. Phys. **1**, 271 (1952).

[31] W. A. Rachinger and A. H. Cottrell, Acta Metall. **4**, 109 (1956).

[32] M. J. Mills and D. B. Miracle, Acta. Met. Mater. **41**, 85 (1993).